Dalton Transactions

An international journal of inorganic chemistry

www.rsc.org/dalton

Volume 40 | Number 32 | 28 August 2011 | Pages 8037–8248

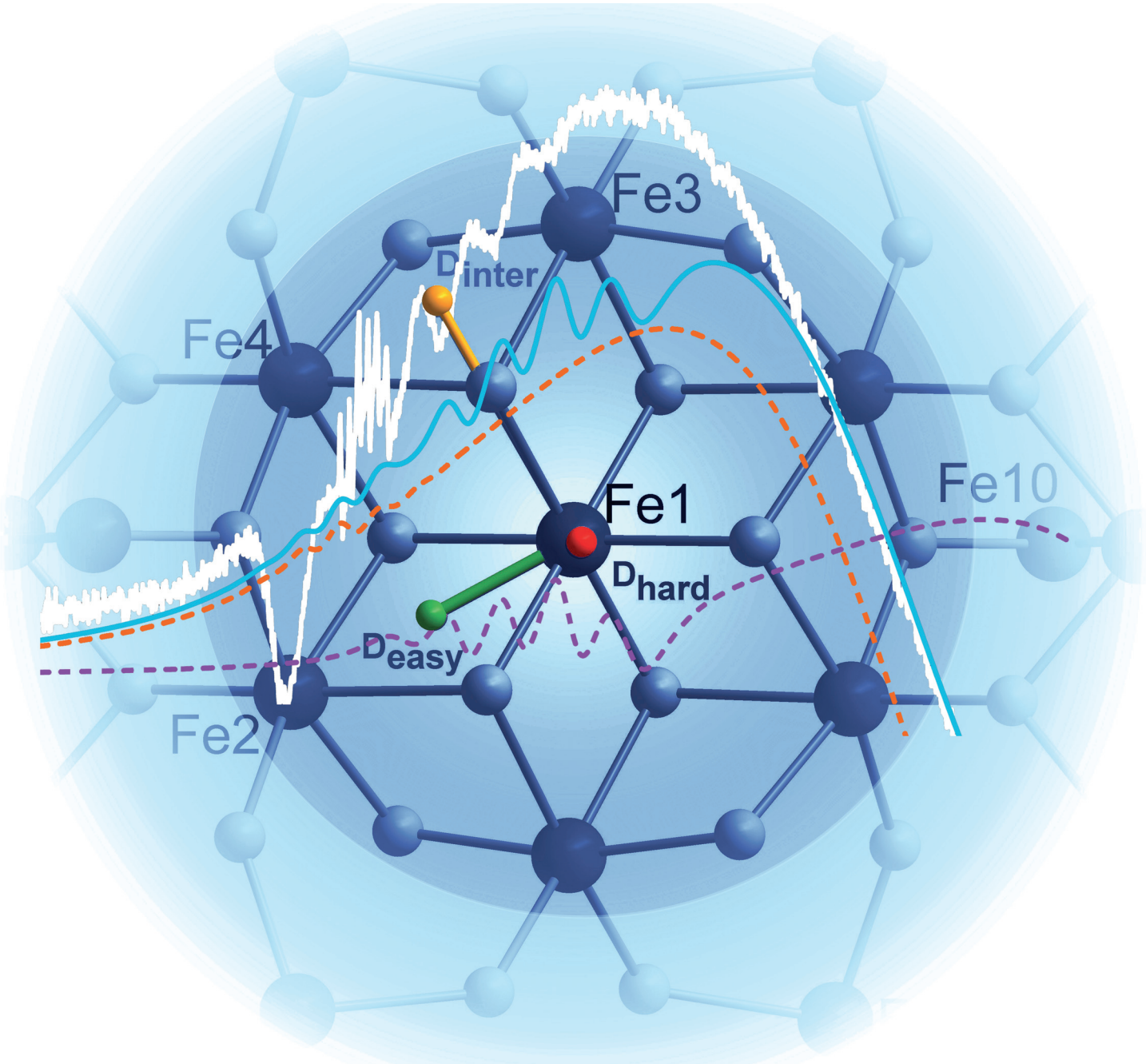

ISSN 1477-9226

RSC Publishing

COVER ARTICLE

Sorace *et al.*

Single crystal EPR study at 95 GHz of a large Fe based molecular nanomagnet

Dalton Transactions

Dynamic Article Links

Cite this: *Dalton Trans.*, 2011, **40**, 8145

www.rsc.org/dalton

PAPER

Single crystal EPR study at 95 GHz of a large Fe based molecular nanomagnet: toward the structuring of magnetic nanoparticle properties†

L. Castelli,[a] M. Fittipaldi,*[a] A. K. Powell,[b] D. Gatteschi[a] and L. Sorace*[a]

Received 23rd February 2011, Accepted 13th April 2011
DOI: 10.1039/c1dt10311c

A W-band single-crystal EPR study has been performed on a molecular cluster comprising 19 iron(III) ions bridged by oxo- hydroxide ions, Fe_{19}, in order to investigate magnetic nanosystems with a behavior in between the one of Magnetic NanoParticles (MNP) and that of Single Molecule Magnets (SMM). The Fe_{19} has a disk-like shape: a planar Fe_7 core with a brucite ($Mg(OH)_2$) structure enclosed in a "shell" of 12 Fe(III) ions. EPR and magnetic measurements revealed an $S = 35/2$ ground state with an $S = 33/2$ excited state lying ~ 8 K above. The presence of other low-lying excited states was also envisaged. Rhombic Zero Field Splitting (ZFS) tensors were determined, the easy axes lying in the Fe_{19} plane for both the multiplets. At particular temperatures and orientations, a partially resolved fine structure could be observed which could not be distinguished in powder spectra, due to orientation disorder. The similarities of the EPR behavior of Fe_{19} and MNP, together with the accuracy of single crystal analysis, helped to shed light on spectral features observed in MNP spectra, that is a sharp line at $g = 2$ and a low intensity transition at $g = 4$. Moreover, a theoretical analysis has been used to estimate the contribution to the total magnetic anisotropy of core and surface; this latter is crucial in determining the easy axis-type anisotropy, alike that of MNP surface.

Introduction

Magnetic nanosystems are attracting strong and growing interest in view not only of the rich fundamental science,[1,2] but also of the many technological applications in which they are involved.[3–13] Nowadays particles of very small dimensions, comprising just hundreds of magnetic ions, can be synthesized. However, the physics governing the properties of small size particles does not fit within a precise framework. Classical mechanics, which is adequate for bigger systems, is inappropriate to explain the manifestation of quantum effects, while a treatment based on quantum mechanics seems unrealistic given the huge dimension of the Hilbert space of these systems.

This dimensional region offers thus the opportunity to investigate what happens at the border between the classical and quantum worlds. To pursue this aim, two approaches are generally followed. One is a bottom-up approach, which searches for the emergence of bulk properties starting from those of the single ions, and is focused on big Molecular NanoMagnets (MNM). The other is a top-down approach, which searches for the change in the properties of the bulk material induced by the dimensional reduction, and is focused on Magnetic NanoParticles (MNP).[1]

So far MNM comprising up to 84 magnetic ions (Mn(III)) have been reported.[14] Iron MNM are of particular importance because the individual building blocks have large magnetic moments. Furthermore, they can be used as models for natural systems like magnetosomes, ferritin, and the recently discovered Dps (*D*NA-binding *p*rotein from *s*tarved cells).[15] In these systems, inorganic cores comprising 10^2 iron ions can be investigated, although the control of the numbers of ions cannot be precise. Moreover, large iron clusters can provide a hint for understanding the growth of inorganic cores in proteins.[16]

In the last decade, many iron(III)-based MNM have been reported, which offer the opportunity of detailed characterization. In many cases studies on single crystals allow getting a deep insight into the magnetic properties of large magnetic clusters in the bottom-up approach. In particular a series of polynuclear iron clusters has been synthesized by using tripodal chelating ligands which create a close packed core that is portion of the brucite ($Mg(OH)_2$) structure enclosed in a shell of Fe/ligand units.[17–19] This series (Fe_7, Fe_{13}, Fe_{17}, Fe_{19}) offers a unique chance to study the structuring of nanoscale properties on increasing the number of interacting magnetic centers.

Here we report a single crystal EPR study at 95 GHz of the $[Fe_{19}(metheidi)_{10}(OH)_{14}(O)_6(H_2O)_{12}]NO_3 \cdot 24H_2O$ cluster (where metheidi is the deprotonated form of *N*-(1-Hydroxymethylethyl)iminodiacetic acid), hereafter Fe_{19}, for which the structure and the magnetic properties of powders were

[a]*Dipartimento di Chimica "U. Schiff" and UdR INSTM, Università di Firenze, Via della Lastruccia 3-13, 50019, Sesto Fiorentino, Italy. E-mail: lorenzo.sorace@unifi.it, maria.fittipaldi@unifi.it*
[b]*Institute of Inorganic Chemistry, Karlsruhe Institute of Technology, D76131 Karlsruhe, Germany*

† Electronic supplementary information (ESI) available. See DOI: 10.1039/c1dt10311c

previously reported.[19,20] This cluster has a brucite like structure for the first two generations of iron ions, the planar Fe_7 core. This last is encapsulated by a shell of 10 ligands, bound to 12 additional Fe(III) ions which are held together in pairs through the dinucleating alcohol arm of the ligand. This arrangement resembles that seen in the iron storage protein ferritin, where nanoparticles of an iron mineral akin to ferrihydrite are encapsulated in a shell of nucleating iron centers and protein ligands.[16] The Fe_{19} molecule is centrosymmetric, with the central iron lying on the inversion center. Furthermore, it shows an approximate C_{2v} symmetry, the pseudo binary axis being oriented along Fe1-Fe3 direction (ref. to Scheme 1). Earlier magnetic characterization[19] suggested a ground state for the cluster of $S = 35/2$, while later results[20] hinted at a ground $S = 33/2$ state. Interestingly, more recent Density Functional Theory (DFT) calculations[21] pointed again to a ground $S = 35/2$ state, indicating that no conclusive evidence about the ground state of the system had yet been reached.

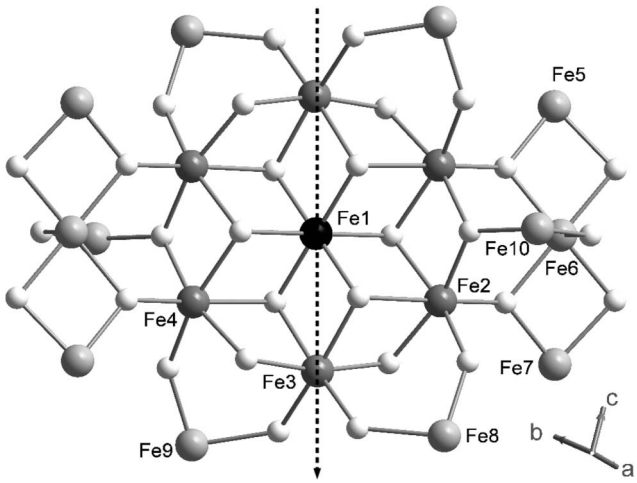

Scheme 1 Sketch of Fe_{19} molecular structure. White: oxygen atoms; the different colors of Fe centers evidence the first (black) and second (dark grey) generation of brucite type lattice as well as the capping centers (light grey). The dashed arrow evidences the pseudo C_2 symmetry axis of the molecule.

Previous EPR measurements on the Fe_{19} complex were limited to powder samples[20] and showed a behavior quite similar to that observed in MNP, the signal becoming more anisotropic on lowering the temperature. Further, spectra were very broad and no fine structure, typical of smaller Fe clusters, was observed. On the basis of the magnetic characterization, the low temperature spectrum was attributed to the $S = 33/2$ ground state. Although the contribution of excited S states was envisaged, this information could not be extracted from the spectra.

The present study was aimed at obtaining a confirmation on the nature of the ground spin state and the fine determination of the magnetic anisotropy, including the orientation of the anisotropy axes, estimated in a previous study on the basis of the pseudo-symmetry of the cluster.[22] The fact that the crystal is triclinic is a disadvantage because the symmetry is low, but it is an advantage because only one set of spectra is observed for each orientation of the magnetic field. The results obtained for Fe_{19} will be compared with those reported in literature for smaller Fe clusters and related to those of iron-oxide based MNP. Indeed, this study on Fe_{19} fits into a wider survey and comparison of magnetic properties of MNM and MNP, which should make it possible to follow the changes imposed by the dimensions, with the final aim of finding a consistent description of the nanosystem properties and behavior.

Experimental

The field dependent magnetization was measured with a Vibrating Sample Magnetometer (Oxford Instruments MAGLAB2000 platform).

The Fe_{19} cluster, synthesized according to the procedure described in ref. 20, crystallizes in the triclinic space group $P\bar{1}$ ($a = 13.309(3)$ Å $b = 17.273(5)$ Å $c = 17.600(4)$ Å $\alpha = 65.201(10)°$ $\beta = 74.514(6)°$ $\gamma = 81.300(2)°$, $V = 3535.8(14)$ Å^3, $Z = 1$). Indexing of a single-crystal of Fe_{19} was performed with X-ray diffraction (XRD) by using an Oxford Diffraction Xcalibur3 diffractometer equipped with Mo-Kα radiation.

X-band and W-band cw-EPR measurements have been performed by using the 9 and 95 GHz Bruker Elexys E500/E600 instrument (Bruker, Rheinstetten, Germany). For both frequencies, a continuous flow He cryostat (Oxford Instruments ESR 900 for X-band and ESR910 for W-band) has been used to obtain low temperatures. The frequency of the field modulation was 100 kHz. The power, the temperature, and the amplitude of the field modulation used to acquire the spectra are specified in the figure captions.

For single crystal measurements in W-band the crystal was mounted on the sample holder, a quartz rod with a diameter of 0.8 mm, by using a NaCl crystal of approximately 0.4 mm of edge. The NaCl cube was fixed on the quartz rod base. For a first rotation (rot. 1), the Fe_{19} crystal was mounted with the *ab*-plane fixed on the top of the NaCl cube, as shown in Fig. 1A. In this configuration, the *ab*-plane is perpendicular to the sample holder axis, which is orthogonal to the external field $\mathbf{B}_0$; therefore, $\mathbf{B}_0$ lies in the *ab*-plane. For a rotation in a different plane (rot. 2), we turned the NaCl cube together with the Fe_{19} crystal by 90°, in a way that the (-1-1-1) plane lay on the base of the quartz rod (see Fig. 1B). For both rotations, the orientation of the Fe_{19} crystal on the NaCl cube was checked again by means of the diffractometer.

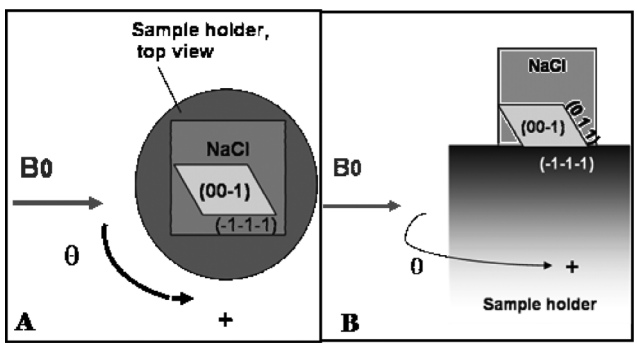

Fig. 1 Crystal configuration on the sample holder in rot. 1 (left) and rot. 2 (right). The angle θ was varied by rotating the sample holder around its own axis, which is perpendicular to the external magnetic field, $\mathbf{B}_0$. The plane containing the iron ions lies on a plane perpendicular to the (00–1) face and parallel to the edge between the (00-1) and the (-1-1-1) face. In rot. 1 the $\theta = 0°$ orientation is represented.

Simulations of the spectra have been performed using the *SIM* simulation software written by prof. H. Weihe.[23] In a first step the zero-field splitting parameters and linewidths for two spin multiplets were varied to obtain a correct reproduction of the resonance fields; later the relative weight of the two multiplets was adjusted to obtain the best simulations at 10 K; this weight was then used to obtain the Boltzmann factors for the two multiplets at the different temperatures allowing to refine the spin hamiltonian and linewidth in order to obtain the best agreement with the experimental data. The field-dependent energy level patterns were drawn using EasySpin Matlab toolbox programmed for EPR simulations.[24]

Results

The field dependence of the magnetization was measured up to 12 T at 1.4, 2.45, and 4.4 K as shown in Figure S1.† Previously reported measurements[20] had been performed up to 7 T. The magnetization value at 1.4 K and 12 T is *ca.* 34.8 μ_B. The new saturation value is in agreement with a ground state $S = 35/2$ with $g = 2$, as suggested by DFT calculations[21] and previously supposed.[19] It is interesting to note that the observed saturation value is equivalent to 65 emu g^{-1} (γ-Fe_2O_3), which compares well with that observed in iron oxide based magnetic nanoparticles grown in a biological reactor,[25,26] lending further support to the need for a common approach to the analysis of the magnetic properties of MNM and MNP.

W-band powder spectra were recorded in the temperature range 10–50 K. The spectra are reported in Fig. 2, together with their simulations, which will be discussed later. At 10 K, the spectrum clearly shows a parallel component at low field, and a perpendicular one at high field. This suggests an almost axial anisotropy, which can be attributed, in first instance, to the zero field splitting (ZFS) of the ground multiplet. The field values at which parallel and perpendicular components occur and their temperature behavior are consistent, as expected, with a dominant easy axis anisotropy. Assuming a simple axial ZFS interaction ($\hat{H}_{ZFS} = D\hat{S}_z^2$) and $g = 2$, and considering $S = 35/2$ as obtained by field dependent magnetization measurements, it is possible to estimate the D value from the powder spectrum spread at low temperature, which, in the high field limit, is equal to $3D(S - 1/2)$. The result, $D \sim -0.027$ cm^{-1}, is in agreement with the D value estimated by Goodwin *et al.* from a high-field EPR powder spectrum recorded at 5 K.[20] On increasing the temperature, the separation between the parallel and the perpendicular components decreases; this is in agreement with the thermal population of levels with smaller values of $|m|$ within the S multiplet(s) in the case of negative D values. Moreover, the intensity of the signal grows around $g \sim 2$ with increasing temperature.

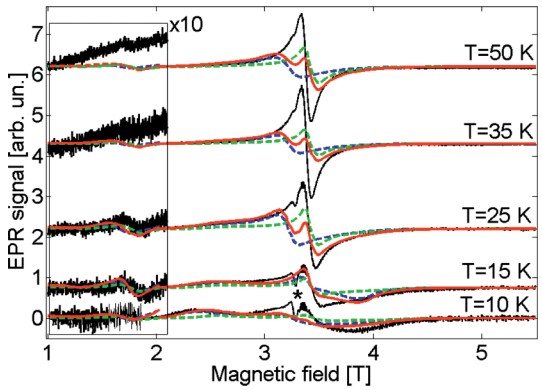

Fig. 2 W-band EPR powder spectra (black) recorded at different temperatures with a microwave power of 15.81 μW and modulation amplitude of 3.00 G. Simulations: contribution of the $S = 35/2$ (blue), contribution of the $S = 33/2$ (green), their weighted sum (red). The asterisk indicates two signals due to paramagnetic impurities in the cavity: a $g = 2$ signal and a Mn sextet, which are present in all the reported spectra.

In order to obtain a more accurate determination of the spin Hamiltonian parameters, a single-crystal EPR study on the Fe_{19} cluster has been performed at 95 GHz. The orientation patterns of rotation 1 and 2 of the EPR spectra, acquired at various temperatures, are reported in Fig. 3, 4 and 5. The orientation dependence of the EPR spectra was recorded by rotating the sample holder about its own axis, which, in rot. 1 (see experimental part), is perpendicular to the *ab*-crystal plane, and thus corresponds to c^* in the crystal reference frame. Since the seven central Fe atoms of the cluster lie in a plane, the normal of which forms an angle of 91.6° with c^*, in this rotation the angle between the normal to the Fe_7-plane and $\mathbf{B_0}$ is varied from 0° to 90° by rotating the sample holder around its own axis. For rot. 1, at 5 K, a minimum of the resonance field is observed at B = 2.30 T and a maximum at 4.00 T. Assuming, in the first instance, axial anisotropy, the direction of $\theta = 0°$ was defined as the one at which the resonance field reaches a minimum at 5 and 10 K. In rotation 1, this direction is reached when the external field is parallel to the edge between the (-1 -1 -1) and the (0 0 -1) face, see Fig. 1A.

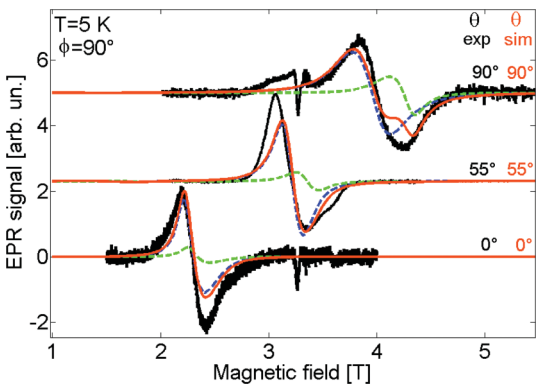

Fig. 3 Single crystal W-band EPR spectra (black) recorded at 5 K and $\phi = 90°$ with a microwave power of 0.05 μW and modulation amplitude of 3.00 G. Simulations: contribution of the $S = 35/2$ (blue), contribution of the $S = 33/2$ (green), their weighted sum (red). On the right, the experimental values of θ are reported in black, while the ones used in the simulations are in red.

In rot. 2, the average Fe_7 plane is parallel to the sample holder base; therefore, the direction of $\mathbf{B_0}$ varies in the Fe_7-plane which coincides, within experimental error, with the average plane of the 19 Fe ions. Of the two extremes in the resonance fields observed for this rotation, the same minimum observed also in the first rotation is obtained, while the maximum occurs at a lower field value than the one observed in rot.1. It is worth noting that the minimum resonance field is observed in both cases for the only common direction probed by the two rotations, *i.e.* the one at the intersection between the two rotation planes (*ab*-plane and Fe_{19}-plane), which corresponds to the Fe1–Fe2 direction. This result

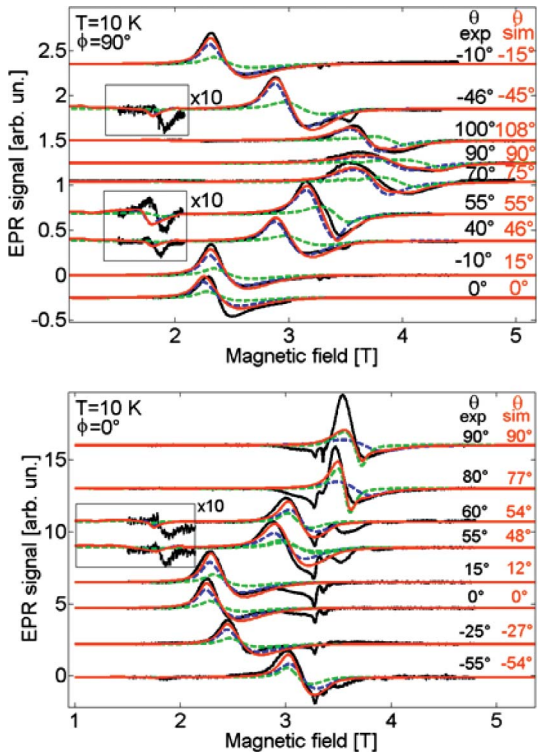

Fig. 4 Single crystal W-band EPR spectra (black) recorded at 10 K with $\phi = 90°$ and a microwave power of 0.5 μW (top) and $\phi = 0°$ and a power of 15.81 μW (bottom), with modulation amplitude of 3.00 G. On the right, the experimental values of θ are reported in black, while the ones used in the simulations are in red. Simulations: contribution of the $S = 35/2$ (blue), contribution of the $S = 33/2$ (green), their weighted sum (red).

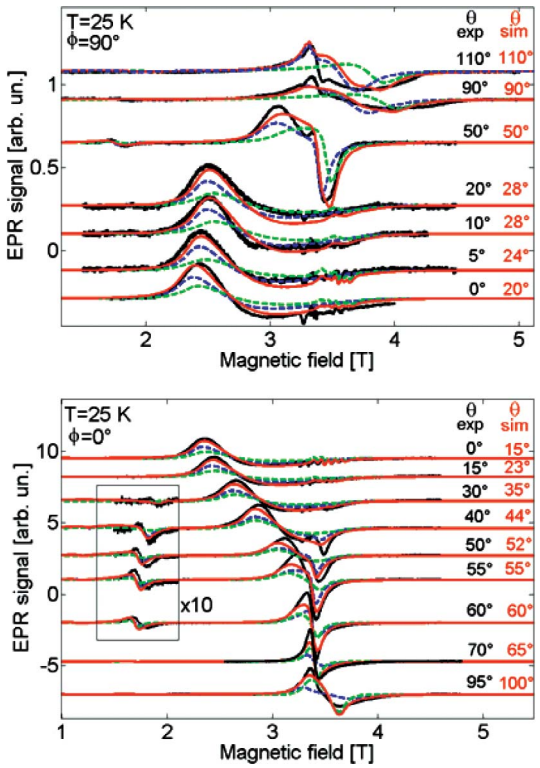

Fig. 5 Single crystal W-band EPR spectra (black) recorded at 25 K with $\phi = 90°$ and a microwave power of 0.5 μW (top) and $\phi = 0°$ and a power of 5 μW (bottom), with modulation amplitude of 3.00 G. On the right, the experimental values of θ are reported in black, while the ones used in the simulations are in red. Simulations: contribution of the $S = 35/2$ (blue), contribution of the $S = 33/2$ (green), their weighted sum (red).

provides a further check on the orientation of the crystal in the two rotations. Furthermore, since a band at the same resonance field is observed also in the powder spectrum, this has to be considered as an absolute minimum, *i.e.* the direction of the easy axis.

Summarizing, the easy axis lies in the Fe_7-plane, along the direction indicated by $\theta = 0°$, and coincides with the Fe1–Fe2 direction, while the intermediate axis is along the line connecting Fe1 with the centre of Fe3–Fe4 (see Fig. 6). This orientation, defined by the two polar angles $(\theta, \phi) = (90°, 0°)$ is obtained when the magnetic field is perpendicular to the (0 0 1) face, that is when the crystal is mounted as shown in Fig. 1B and the magnetic field is perpendicular to the paper plane.

Following these results, our reference frame is such that in both rotations the value of θ is varied, while ϕ is fixed ($\phi = 90°$ in rot. 1 and $\phi = 0°$ in rot. 2); further the angle θ indicates the angle between the easy axis and $\mathbf{B}_0$. After a complete rotation (360°) the same spectrum is obtained within 8°, which is thus assumed to be the experimental error affecting the nominal θ values. The error on ϕ is minimized by the mounting procedure.

Generally, the spectra do not show the well resolved fine structure typical of smaller Fe clusters; rather, a broad resonance is observed, the width and resonance field of which show strong temperature and orientation dependence. We attribute this to the convolution of transitions separated by field values which are smaller than twice their linewidth,[27] thus resulting in a single broadened line. For $\theta = 0°$, the separation between two transitions of the $S = 35/2$ multiplet is expected to be about 640 G for the

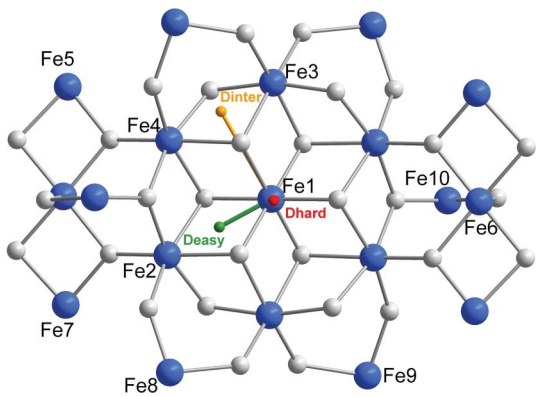

Fig. 6 Experimentally determined orientation of the Zero Field Splitting tensor of the $S = 35/2$ state of Fe_{19} in the molecular frame. Light blue: iron atoms; grey: oxygen atoms.

estimated $|D|$ of 0.03 cm^{-1}, pointing to a linewidth larger than 320 G. For rotation 1, the resonance field varies from ~2.30 T to ~4.00 T at 5 K, from ~2.43 T to ~3.95 T at 10 K, from ~2.60 T to ~3.65 T at 25 K. In agreement with the temperature behavior of the spectrum spread observed in the powder sample, the resonance field variation is larger at lower temperatures. The same trend is observed also for rot. 2. This behavior is due to the easy axis type anisotropy: indeed, on lowering the temperature, levels characterized by larger $|m|$ values are increasingly populated, and

their resonance fields are the furthest from the field corresponding to the free electron g value (see eqn (1) below).

In the spectra recorded at 10 K with $\theta \sim 90°$ and $\phi \sim 90°$ and in those at 25 K with $\theta \sim 0°$, a partially resolved fine structure is observed, the position of which is orientation dependent (Fig. 7 and 8). Moreover, a half field band, which is also present in powder spectra, is observed at 10 and 25 K, being more pronounced at the latter temperature. Further, its intensity is higher at about 50° from the easy axis, in agreement with the prediction of the theory,[28] $\theta_{max} = 45°$, therefore confirming our axis assignments. At 25 K, at orientation close to 50° another interesting feature of the spectra occurs: a sharp component at approximately $g = 2$, which is also present in the powder spectra.

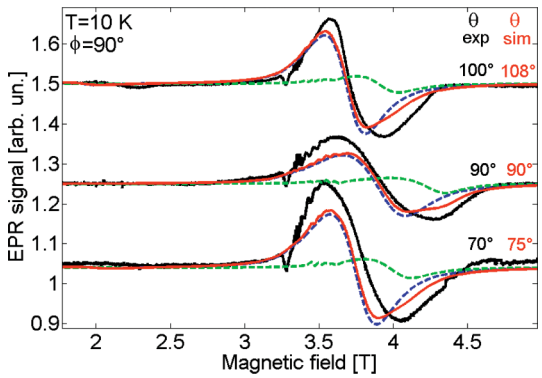

Fig. 7 W-band EPR spectra (black) of a single crystal of Fe_{19}, around $\theta = 90°$ and at $T = 10$ K. Simulations: contribution of the $S = 35/2$ (blue), contribution of the $S = 33/2$ (green), their weighted sum (red). On the right, the experimental values of θ are reported in black, while those used in the simulations are in red.

X-band powder spectra in the temperature range 5–290 K have been also acquired and they are shown in Fig. 9. Very broad spectra extending approximately on the whole field range are observed with apparent resonant field decreasing on decreasing temperature.

Analysis of the EPR spectra

Global angular dependence of the spectra

In the analysis of the spectra we started from the simplest possible approximation, the so called giant spin approximation, *i.e.* calculating only the transitions within the ground state $S = 35/2$, and we included only second order zero field splitting effects. For axial anisotropy and isotropic g, in the high-field approximation, *i.e.* assuming that the Zeeman energy is larger than the zero-field splitting one, the resonance field corresponding to the transition between levels m and $m+1$ is given by the relation:[29]

$$B_r(m \rightarrow m+1) = \frac{g_e}{g} \cdot B_e - \frac{D}{g\mu_B} \cdot \frac{2m+1}{2}(3\cos^2\theta - 1) \qquad (1)$$

where g is the Landè factor, g_e is the free electron g-value, B_e its corresponding resonance field, and μ_B is the Bohr magneton. Since in W-band the ratio between the Zeeman energy at field corresponding to g_e and the quantity SD is of the order of 10, expression (1) is in principle suitable to describe the global angular behavior of B_r. According to relation (1), when $D < 0$ (easy axis

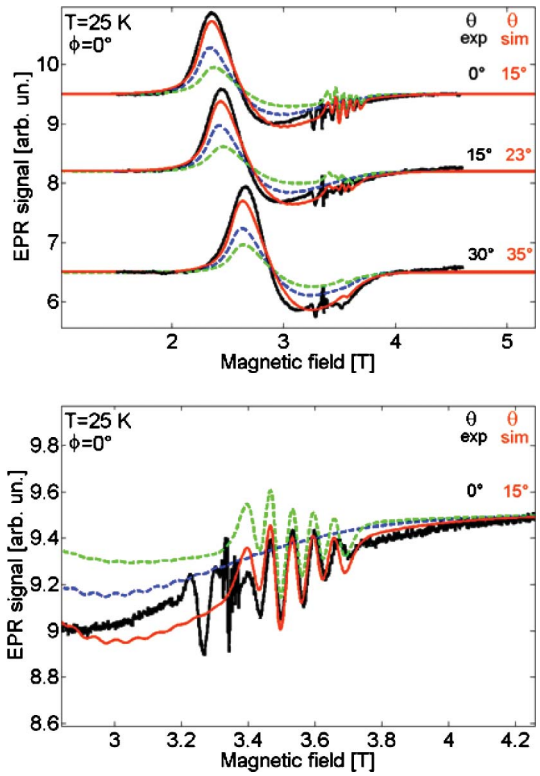

Fig. 8 Upper panel: W-band EPR spectra (black) of a single crystal of Fe_{19}, around $\theta = 0°$ and at $T = 25$ K. On the right, the experimental values of θ are reported in black, while those used in the simulations are in red. Simulations: contribution of the $S = 35/2$ (blue), contribution of the $S = 33/2$ (green), their weighted sum (red). Lower panel: enlarged area of W-band EPR spectrum (black) of a single crystal of Fe_{19}, corresponding to $\theta = 0°$.

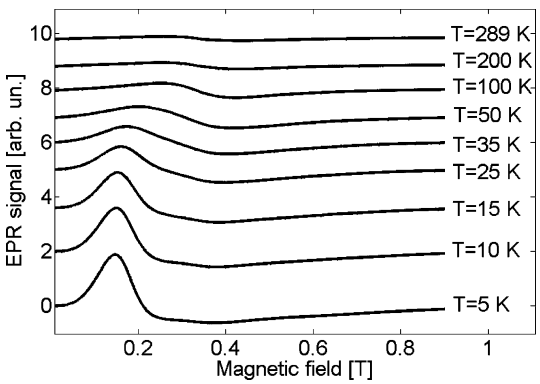

Fig. 9 X-band EPR powder spectra of Fe_{19} at different temperatures with a microwave power of 65.57 μW.

anisotropy) for levels with $m < 0$ the minimum in B_r corresponds to $\theta = 0°$, while the maximum is reached when $\theta = 90°$. Moreover, at $\theta = 54.7°$ (magic angle) all the transitions collapse at a field value corresponding to the g value of the system, because the magnetic anisotropy of the second order axial Zero Field Splitting is cancelled. The spectra acquired at this angle will thus be sharper. This 'singular condition' can be identified also in the powder spectra where the clusters with easy axes lying on the conic surface corresponding to $\theta = 54.7°$ give a sharp contribution to the spectra at $g = 2$. In ideal cases, clusters with orientation different from

θ = 0° and θ = 90° do not give rise to signals in derivative spectra of powder samples, since no stationary points are present in the absorption at these angular values. However, in this case the coalescence of all the transitions at $\theta \approx 54.7°$ causes an effective stationary point in the angular dependence of the resonance fields (Fig. S2†), which gives rise to a sharp signal at $g = 2$; a similar effect was reported by some of us in the analysis of a tetranuclear iron(III) single molecule magnet.[30] Moreover, the correlation between the narrow feature and the magic angle orientation is supported by the experimental temperature behavior, that is the increase of the sharp signal intensity on increasing temperature. This trend is indeed supported by the energy diagram of the spin ground state S = 35/2 calculated at $\theta \approx 54.7°$ (Fig. S3†), which shows the presence of coincident transitions around $g = 2$, acquiring intensity at higher temperature.

Full simulation of the spectra

Since only an average resonance field of levels with different $m <$ 0 values is observed in the spectra, eqn (1) could be used only to provide a rough estimate of $D \sim -0.026$ cm^{-1} as well as providing initial estimate on the principal axis orientations. In a further step, a more complete spin Hamiltonian[29] including rhombic terms was considered to analyze and simulate the temperature and orientation dependence of the EPR spectra:

$$\hat{\mathbf{H}} = g\mu_B \hat{\mathbf{S}} \cdot \hat{\mathbf{B}} + D\left[\boldsymbol{S}_z^2 - \frac{1}{3}S(S+1)\right] + E(\boldsymbol{S}_x^2 - \boldsymbol{S}_y^2) \qquad (2)$$

where E is the rhombic parameter of the ZFS. The necessity of including this last contribution clearly emerged from the inspection of the two rotation patterns: in rot. 1 the maximum occurs at a higher field value than in rot. 2, indicating the presence of two directions with different magnetic properties in the hard plane. Higher order terms were not included to avoid overparametrization of the system, since its low symmetry would result in the inclusion of at least three 4th order terms with principal directions arbitrarily oriented.[31] It was immediately evident that it is not possible to reproduce the experimental shapes and exact field positions by considering only the spin ground state $S = 35/2$, even for the lowest temperature spectra. The asymmetry of the line shapes, the fact that they are very broad especially at orientations around $\theta = 90°$, the emergence of a partially resolved fine structure at particular temperature and orientations (see Fig. 7 and 8), could be reproduced only by considering the contribution of an excited state with $S = 33/2$, with different Spin Hamiltonian parameters. The ratio between the contribution to the simulated spectra of the S = 35/2 and S = 33/2 at T = 10 K needed to reproduce the experimental ones was used to estimate the energy separation between the two levels ($E_g \sim 8$ K), assuming Boltzmann-distributed populations.

The parameters used to simulate the spectra are reported in Table 1. Isotropic g-tensors were used for both spin states, since Fe(III) has an orbital singlet state; moreover, the same principal axis orientations of the ZFS tensors were assumed for the two states. The rhombic character of the ZFS of the S = 33/2 state is larger than that of the S = 35/2 ground state. This proved necessary to reproduce the broad spectra at orientation close to the hard axis; however, the same effect could have been in principle produced by the inclusion of higher order transverse terms in the Hamiltonian, the absence of which might also explain the low value of g obtained for the excited state. Moreover, a sizeable strain of the ZFS parameters had to be used: indeed, a simple larger linewidth, although anisotropic, did not reproduce the orientation dependence of the lineshape, which is narrower around θ = 55°, *i.e.* close to the magic angle. As mentioned above, at this angle the ZFS contribution cancels and so does the corresponding strain, resulting in a peculiar sharpness of the spectrum. The simulated spectra are reported together with the experimental ones in Fig. 3–5.

Table 1 Hamiltonian parameters for the ground state (S) and first excited state (S_{exc}) and their energy separation (E_g) for the clusters Fe_4, Fe_7, Fe_8, Fe_{11}, and Fe_{19}

	Fe_4	Fe_7	Fe_8		Fe_{11}	Fe_{19}	
S, S_{exc}	5[a]	5/2[b]	10[c]	9[d]	13/2[f]	35/2	33/2
E_g ($S_{exc} - S$) (K)			24[d]			8	
D (cm^{-1})	−0.421[a]	−0.43[b]	−0.21[c]	−0.19[d]	−0.25[f]	−0.03	−0.032
$\sigma_D/\lvert D\rvert$	0.029[a]		0.01[1,e]			0.07	0.06
E/D	0.05[a]		0.2[c]	±0.18[d]		0.05	0.19
$\sigma_E/\lvert E\rvert$	1.71[a]					3.33	0.17
g_{iso}	2.0[a]					2.0	1.97
$\lvert D\rvert S^2$ (K)	12.2[a]	3.9[b]	30[c]		15[f]	13.2	12.5

[1]Contribution of intercluster dipolar interactions not included. [a] Ref. 34 [b] Ref. 17 [c] Ref. 35 [d] Ref. 36 [e] Ref. 37 [f] Ref. 38

The value of θ used in the simulation was allowed to vary within the estimated experimental error, which is 8°. The nominal experimental value is reported in the figures together with the value used in the simulation. The discrepancy between these two values is within 8° for temperatures up to 10 K, while it is larger at higher temperatures, although the experimental error is the same. This may originate from the contribution of higher excited states, not included, which are expected to be characterized by a different magnetic anisotropy. This could explain why the discrepancy in the θ values is more evident for angles close to θ = 0°, where the resonance field is more sensitive to the magnetic anisotropy (assuming the same orientation of the principal axes of the ZFS tensors for different spin states).

The calculated spectra reproduce quite well the experimental orientation dependence, the agreement being more pronounced at lower temperature than at higher ones. As the temperature increases there are parts of the experimental spectra that cannot be simulated by considering only the spin states S = 35/2 and S = 33/2. We attribute also these discrepancies to contributions from higher lying excited states, which are beyond the simple model considered here. Indeed, considering the estimated energy separation $E_g \sim 8$ K between the ground state and the first excited state, and the strongly "frustrated" nature of the exchange interactions characterizing Fe_{19},[19–21] it appears reasonable that higher spin states are populated even at relatively low temperature as 25 K.

Remarkably, the fine structure observed in the spectra acquired at 10 K with (θ, ϕ) ~ (90°, 0°) and at 25 K with $\theta \sim 0°$ could be nicely reproduced by the simulations (Fig. 7 and 8), making it possible to attribute them to single transitions between energy levels with small $|m|$ values of the excited $S = 33/2$ state. However, these experimental features could not be correctly reproduced by assuming the same linewidth for all the transitions and it was found that a smaller linewidth (from 2 to 5 times smaller than that

used for the remaining ones) attributed to the transitions of the observed structure largely improved the quality of the simulations. To correctly reproduce the total width of the experimental spectra, the linewidth was modeled according to the following relation:

$$\Delta B(S,m,T,\theta) = \Delta B_0(S,m,T,\theta) + \sigma_D \left|\frac{\partial B}{\partial D}\right| \quad (3)$$

where the first term of the sum accounts for the temperature dependence of the linewidth, and the second one accounts for the broadening of the transitions between levels with large $|m|$ value. σ_D is the D-strain parameter and $|\partial B/\partial D|$ obviously depends on both m and θ. The orientation dependence of this second term is also responsible for the sharp spectra obtained close to the magic angle where, as mentioned above, the effect of ZFS is cancelled and the broadening due to the D-strain is not effective.

Due to the large number of transitions included in the spectra and to the contribution of the strain, it is difficult to estimate the ΔB_0 contribution for each transition. Furthermore, ΔB_0 variations produce only small modifications in the spectrum shape and therefore this parameter can not be accurately determined by this analysis, especially for low temperature spectra. At higher temperature the contribution of transitions between states with small |m| value, less affected by the strain, is larger, leading to an easier determination of ΔB_0. However, the indetermination in the ΔB_0 value is quite large even at 25 K (ΔB_0 can be varied up to 300 G without producing significant changes in the spectral shape), while it is reduced for the bands of the resolved fine structure, in which an increase of 200 G in the ΔB_0 parameter causes the disappearing of the resolved transitions. For these particular features is thus possible to follow the dependence of ΔB_0 on m, which is reported in Fig. S4 and Fig. S5.†

The ΔB_0 values used in simulations decrease on decreasing temperature; this would be in agreement with the expected increase of relaxation times. However, due to the relatively large indetermination on this parameter at lower temperatures, this trend has to be considered with caution.

The Hamiltonian parameters obtained from the analysis of single crystal data were subsequently used to simulate the powder spectra (Fig. 2). It is evident that the agreement between the experimental spectra and the simulation becomes worse at higher temperatures, again confirming the likely presence of low lying excited states contributing to the EPR spectrum, as well as the possible breakdown of the Giant Spin Model approach at higher temperatures.[32,33] Indeed, deviations from strong exchange limit which result in a mixing among low-lying states are usually modeled by higher order terms in the Giant Spin Hamiltonian, which were not included in our study.

Finally, the simulations of the X-band powder spectra of the Fe_{19} with the Hamiltonian parameters derived from the 95 GHz analysis are reported in Fig. S6.† The simulations fail to reproduce the experimental spectra especially in the low field part of the spectrum even at 5 K, while the high field part of the spectrum is quite well reproduced. The reason for this can be understood by analyzing the field dependent energy pattern of the m sub-levels for the ground $S = 35/2$ state. It is evident that in X-band the transitions occurring at low fields originate from levels quite high in energy, corresponding to small values of |m|, which are quite close in energy to each other (Fig. S7 and Fig. S8†). This most probably results in a broadening of the corresponding lines beyond detection. On the contrary, in W-band, transitions occur between levels which are always well separated in energy (Fig. S9 and Fig. S10†). For temperatures higher than 15 K, the disagreement between experimental and simulated X-band spectra derives also from the contribution of S-multiplets higher in energy, similarly to what is observed in the W-band spectra.

Discussion

Comparison with other iron-based molecular nanomagnets

The experimental spectra can be reasonably well reproduced by considering the contribution of two S states, separated by an energy gap of $E_g = 8$ K, which is smaller than the energy barrier corresponding to the S ground state ($|D|S^2 = 12$ K), suggesting that a partial breakdown of the single-spin model might occur. At temperatures higher than 10 K, higher lying excited states seem to contribute to the spectra, as witnessed by the increasing discrepancies between experimental and simulated spectra with increasing temperature.

For the two lowest lying spin states, the directions of the easy axes of the ZFS tensors are found in the Fe_{19}-plane along the Fe1–Fe2 direction, while the hard axes are perpendicular to it. For both S states, the rhombic parameter E is relevant, being larger for the excited $S = 33/2$ state.

In Table 1, the Hamiltonian parameters and E_g known for several Fe-clusters are reported, in order to facilitate the comparison.[17,34–38] Increasing the number of the Fe ions results in a decrease of both E_g and $|D|$, so that Fe_{19} has the smallest values of $|D|$ and E_g of the series. We have shown recently that the example of the ring systems, which can be treated analytically, allows a rationalization of these trends on the basis of some simplifying assumptions (*i.e.* ferromagnetic interactions and collinear single ion anisotropy axes).[1] The E_g and $|D|$ values reported in Table 1 do not follow exactly the predicted trend since in the considered cluster the ground state results from dominating antiferromagnetic interactions and the single ion anisotropy axes are far from being collinear.

Finally, we consider it important to discuss the variation of the ratio $\sigma_D/|D|$ when the number of Fe ions is increased. It should be noted that in the present analysis, as well as in that of Fe_4 clusters,[34] the m dependence of the line broadening has been modelled by an effective D-strain, which actually accounts for the effects of two distinct contributions: single cluster D-strain and inter-cluster dipolar interactions.[37] Since the first contribution depends on the same parameters as the cluster D values (single ion and intra-cluster dipolar contribution), it is expected to scale approximately in the same way on varying the dimension of the clusters, and it should then not provide any definite trend of $\sigma_D/|D|$. On the contrary, the variation of intercluster dipolar contribution, which in our treatment is included in the global σ_D parameter, might explain the large value of the ratio $\sigma_D/|D|$ observed for Fe_{19} compared to the smaller Fe_4.‡ Indeed, this interaction is expected to be larger in the former nanomagnet,

‡ We also note that the use of phenomenological strain parameters can be the reason of the anomalous value of σ_E which had to be introduced in the first excited state in order to reproduce the spectral shape.

since the intercluster distance is comparable to that of Fe_4 while the spin value is much larger. In agreement with this, an estimate of the dipolar energies using the relation $E_{dip} = Z(g\mu BS)^2/V$ (where Z is the number of molecule per unit cell and V is the cell volume) provides $E_{dip}(Fe_4) = 25$ mK and $E_{dip}(Fe_{19}) = 190$ mK.[22] On the basis of these results a higher resolution of the EPR spectrum might in principle be obtained by performing the EPR experiments at even higher magnetic fields, where the contribution of the intercluster dipolar interactions should produce a less significant effect.[37]

Features relevant for MNP spectra

Observation of fine structure resolved transitions in EPR spectra of Fe_{19}, at particular angles and temperatures, is an important result, indicating that this system shows a magnetic behavior that is intermediate between that of smaller clusters and that of MNP.

The sharp feature present at 25 K near $g = 2$ in both single crystal and powder spectra of Fe_{19}, which has been already discussed in the previous section, can help in the understanding of Electron Magnetic Resonance (EMR) spectra of MNP. Indeed, a similar spectral feature is generally observed at high temperatures in the (EMR) spectra of small Fe-based MNP,[39,40] and its origin is still debated.[41–43] The present study suggests that it can be attributed to the contribution of nanomagnets, either MNM or MNP, with an 'orientation singularity', *i.e.* with the easy axes oriented at the magic-angle with respect to the external field. Another interpretation based on the decoupling between surface and core spins has been discussed elsewhere.[26,44]

A second relevant feature which is present in the spectra of both Fe_{19} (single crystal and powder) and MNP is a half-field signal, the intensity of which decreases upon decreasing the temperature. In MNM, this resonance acquires intensity through admixing of the adjacent states m ±1 due to the non-diagonal matrix elements of the operators $\hat{S}_z\hat{S}_\pm$ in the Spin Hamiltonian.[28] These are due to the non coincidence between the external magnetic field and the easy axis, for axial anisotropy, and also from the rhombic term of the ZFS. This admixing allows otherwise formally forbidden transitions with $\Delta m = \pm 2$. The same origin has been attributed to the half field resonance in MNP with axial anisotropy, which thus points out the discreteness of energy levels also in these systems.[26,42,45] For MNP with uniaxial anisotropy, the intensity of the half-field signal is expected[42] to be maximum at $\theta = 45°$. Moreover, in powder spectra, the broadening of this signal parallels that of the major signal. For Fe_{19} as for MNP, the major signal of the spectrum broadens upon lowering the temperature and so does the half-field resonance.

Rationalization of the anisotropy

In the strong-exchange limit[46] the observed anisotropy of the S multiplet of an exchange coupled cluster can be related to the parameters of each paramagnetic center, s_i, of the cluster, through eqn (4):

$$\mathbf{D}_S = \Sigma_i d_i \mathbf{D}_i + \Sigma_{ij} d_{ij} \mathbf{D}_{ij} \quad (4)$$

where for the sake of simplicity, we did not consider the antisymmetric contribution to the anisotropy. In eqn (4), $\mathbf{D}_i$'s are the single ion Zero Field Splitting tensors, $\mathbf{D}_{ij}$'s are the tensors describing the pairwise interactions, both through space (dipolar anisotropy) and through bond (exchange anisotropy), d_i's and d_{ij}'s are projection coefficients which can be calculated through recursive formulae once the composition of the wavefunction of S in terms of each single spin is known. Since this piece of information is not available for Fe_{19}, due to the huge dimension of its Hilbert space ($6^{19} \times 6^{19}$), we chose the coupling scheme described in ref. 19 on which the estimation of a ground state $S = 35/2$ was based (see Scheme 2). The dipolar contribution calculated on the basis of this coupling scheme by considering all the 171 pairwise interactions of the Fe_{19} cluster turned out to be close to the complete rhombic limit ($E/D = 1/3$), with the easy axis oriented in the iron plane along the Fe1–Fe3 direction (pseudo C_2 symmetry axis), and the intermediate axis coincident with the perpendicular to the iron plane (Fig. 10). It is interesting to note that by using different coupling schemes the rhombic character of the dipolar contribution is preserved, as well as the direction of one of its principal axis along the normal to the iron plane. On the other hand, some rotation (up to 15°) of easy and hard axes, lying in the iron plane, is calculated depending on different coupling schemes. For all the coupling schemes investigated, the absolute value of the calculated dipolar contribution accounts for about half of the experimentally determined anisotropy. This is about halfway between the results obtained for Fe(III) based antiferromagnetic rings (for which dipolar contribution may explain virtually all the anisotropy[47]) and smaller high spin clusters for which the single ion contribution was thought,[48] and then found,[49] to be dominant. Indeed, for tetranuclear iron clusters with a propeller shape characterized by an $S = 5$ ground state, the calculated dipolar contribution is oriented in the right direction and has the correct sign, but its magnitude is only a tenth of the global anisotropy. For Fe_8 cluster, the calculated dipolar tensor is different in sign, magnitude and orientation from the experimentally determined one (with the exception of intermediate axis, which is well reproduced), so that, even in this case, large contribution of single ion anisotropies to the global one has been supposed.[50]

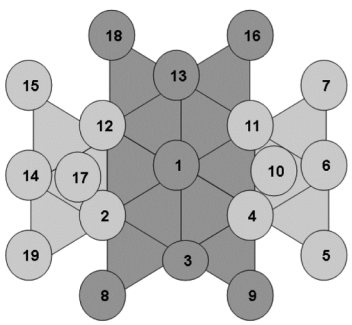

$S_5 + S_6 + S_7 + S_{10} = S_A = 10.$

$S_4 + S_{11} = S_B = 5.0$

$S_A + S_B = S_{AB} = 5.0$

$S_{14} + S_{15} + S_{19} + S_{17} = S_C = 10.$

$S_2 + S_{12} = S_D = 5.0$

$S_C + S_D = S_{CD} = 5.0$

$S_3 + S_8 = S_E = 0.$

$S_E + S_9 + S_1 = S_F = 5.0$

$S_F + S_{13} + S_{16} + S_{18} = S_G = 15/2$

$S_{AB} + S_{CD} = S_{ABCD} = 10.0$

$S_{ABCD} + S_G = S_{tot} = 35/2$

Scheme 2 Sketch of the tripartite coupling scheme used to derive the projection coefficients of single ion and dipolar tensors for the $S = 35/2$ ground state.

The estimation of the latter contribution for Fe(III) based clusters is however not obvious, in the absence of dominant and well identified distortions from pure octahedral symmetry.[51] Previous results on smaller clusters[48,50,52] have indeed demonstrated that, while the single ion anisotropy may reach a value as high as

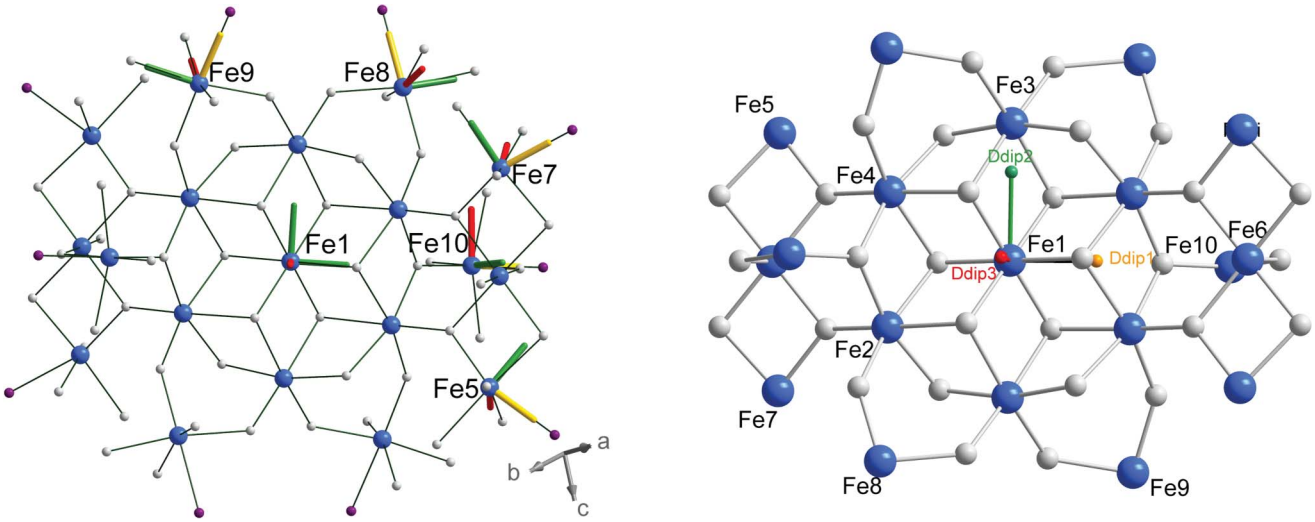

Fig. 10 Orientation of the calculated single-ion Zero Field Splitting tensors (left) and of the global dipolar contribution (right) with respect to the molecular structure of Fe_{19}. Single-ion tensors not shown for Fe2, Fe3 and Fe4, due to their small magnitude. Light blue: iron atoms; grey: oxygen atoms; purple: nitrogen atoms. Green, orange and red rods evidence the orientation of easy, intermediate and hard axes of each calculated tensor.

0.7 cm^{-1}, a quantitative estimation of this value on the basis of the coordination properties of Fe(III) centers is not straightforward. In this respect, ligand field based models were partially successful, being able to provide some qualitative information at least on sign and magnitude of single-ion anisotropy.[48,53] For this reason we proceeded to an estimation of single ion contribution of each of the 10 crystallographically distinct iron centers, by using an Angular Overlap Model based program.[54] A first point to be noted is the remarkable similarity of the coordination spheres - and thus of their expected single ion anisotropy - of the outermost iron(III) centers, (Fe(i), i = 5,6, . . . ,10) characterized by an approximate C_{2v} point symmetry with two *trans* oxygens making an angle of 155° and each Fe–N direction identifying the local pseudo binary axis. This results in an estimated single ion contribution of $|D| \approx 0.5$ cm^{-1} and strongly rhombic character (E/D *ca.* 0.3), with the pseudo C_2 symmetry axis of the center being the intermediate axis (see Fig. 10 for orientation of the calculated single-ion anisotropy tensor). Another center which is estimated to possess relevant single ion anisotropy is the central one, Fe1. Its coordination geometry is easily identified as a trigonally compressed octahedron, with the angle characterizing the distortion being about 60° (compared to 54.73° for a regular octahedron). This makes the value expected for D positive and quite large (D = +0.5 cm^{-1}), with the hard axis oriented along the pseudotrigonal axis (*i.e.* the perpendicular to the Fe_7 plane).[55] Finally, the contribution of Fe2 (and thus of Fe4, due to the similarity of their coordination sphere) and Fe3 is estimated to be much smaller ($|D| < 0.1$ cm^{-1}).

On the basis of these results, and by using the calculated projection coefficients obtained from the coupling scheme sketched in Scheme 2, the global estimation of the single ion contribution to the anisotropy is of the correct order of magnitude compared to the experimental one ($|D| \approx 0.01$ cm^{-1}). However, at variance with dipolar contributions, its orientation appears to be strongly dependent on the coupling scheme chosen, thus resulting in different results for the calculated global anisotropy. While this confirms the significant difficulties in estimating the anisotropy of large iron(III) based clusters from simple models, it also indicates that the assumption of C_{2v} symmetry for the cluster is an oversimplification, and large deviation (as those observed experimentally) from the idealized symmetry can be expected. Further, it has to be considered that the exchange anisotropy contribution, which is usually neglected in iron(III)-containing centers on the basis of Moriya approximation,[56] has been recently shown to be of magnitude comparable to that of the dipolar interaction.[57,58]

A final issue which is worth discussing here concerns the different contributions from "core" ions (Fe_7 plane) compared to the anisotropy induced by the "surface" ions, which, together with ligands, are blocking the growth of the brucite type lattice. Such an analysis might be of interest in the comparison of the magnetic properties of MNM with MNP. It turned out that both dipolar contribution and single ion ones due to the Fe_7 core are -as expected on the basis of symmetry considerations- much less rhombic than the corresponding tensors obtained when considering all the 19 Fe centers (see Table 2). The two calculated contributions are of comparable magnitude and both of hard axis type ($D > 0$), the axis being oriented along the normal to the core plane. The estimate of the contribution of the "surface" ions to the global anisotropy is less simple, due to the lower point symmetry of the Fe(III) centers and the large uncertainty on the projection coefficients. However, considering that the experimental characterization clearly indicates that the normal to the core plane is a hard axis for Fe_{19} but the cluster features an easy axis type anisotropy, the contribution of "surface" ions (both dipolar and single ion) has to be assumed as the dominant one in determining the global anisotropy of the cluster.

Conclusions

We have shown that even for large molecular clusters, for which the powder EPR spectra is characterized by unstructured broad lines, the intrinsic higher resolution/selectivity of single crystal measurements make it possible to observe a partially resolved fine structure in the EMR spectra and to disentangle the contributions

Table 2 Comparison of the calculated dipolar (D_{dip}) and single ion (D_{SI}) contribution to the global zero field splitting of $S = 35/2$ state considering either all the 19 iron ions Fe_{19} or only the planar Fe_7 core (values in cm^{-1}). The tensors are expressed in a reference system providing a diagonal experimentally determined tensor, the values of which are reported in the last column (Z is directed along the perpendicular to the Fe_7 plane and X along Fe1–Fe2 direction)

	$D(Fe_{19})$	$D(Fe_7)$	$D_{dip}(Fe_{19})$	$D_{SI}(Fe_{19})$	$D_{SI}(Fe_7)$	$D_{dip}(Fe_7)$	D_{exp}
D_{XX}	-1.28×10^{-2}	-3.7×10^{-3}	-1.06×10^{-2}	-2.2×10^{-3}	-1.3×10^{-3}	-2.4×10^{-3}	
D_{YY}	$+1.21 \times 10^{-2}$	-1.2×10^{-3}	$+1.22 \times 10^{-2}$	-1×10^{-4}	-1.0×10^{-3}	-2.0×10^{-4}	
D_{ZZ}	$+ 6 \times 10^{-4}$	$+5.0 \times 10^{-3}$	-1.6×10^{-3}	$+2.3 \times 10^{-3}$	$+2.3 \times 10^{-3}$	$+2.6 \times 10^{-3}$	
D_{XY}	-3.1×10^{-3}	$+1 \times 10^{-4}$	$+5 \times 10^{-4}$	-3.6×10^{-3}	$+1.0 \times 10^{-4}$	0	
D_{XZ}	-6×10^{-4}	0	-1×10^{-4}	-5×10^{-4}	0	0	
D_{YZ}	-2.1×10^{-3}	0	-1.3×10^{-3}	-8×10^{-4}	0	0	
D_1	-1.31×10^{-2}	-3.7×10^{-3}	-1.06×10^{-2}	-4.4×10^{-3}	-1.3×10^{-3}	-2.4×10^{-3}	-2.1×10^{-2}
D_2	$+3 \times 10^{-4}$	-1.3×10^{-3}	-1.7×10^{-3}	$+3.7 \times 10^{-3}$	-1.1×10^{-3}	-2.0×10^{-4}	$+4.5 \times 10^{-3}$
D_3	$+1.28 \times 10^{-2}$	$+3.1 \times 10^{-3}$	$+1.23 \times 10^{-2}$	$+7 \times 10^{-4}$	$+2.4 \times 10^{-3}$	$+2.6 \times 10^{-3}$	$+1.65 \times 10^{-2}$

of an excited S state already at 5 K. Furthermore, the single crystal analysis provided both the magnitude of the Zero Field Splitting tensors of the two lowest spin states and their orientation with respect to the molecular frame. In turn, this information was used to estimate by means of a simple model the different contributions to the global magnetic anisotropy, allowing us to trace differences and similarities with both smaller clusters, with well understood EPR properties, and MNP, for which the comprehension of the EMR behavior is still problematic. In this respect, it has to be considered that the small energy gap observed between the two low lying states is expected to further decrease upon increasing the dimension[1] of the cluster, going towards a continuum of states which is closer to what most likely occurs in a MNP. It is thus clear that to obtain meaningful and reliable information on EMR spectra of large clusters the use of orientation dependent single-crystals is required. However, it has to be noted that, since on increasing the cluster size the energy separations (exchange constant and ZFS parameters) are expected to decrease,[1] the resolution issue will become even more demanding, with the linewidth of the transitions being the critical parameter.

Finally, the estimation of the different contributions to the magnetic anisotropy of the Fe_{19} indicates that the "surface" ions are the dominant ones in determining the global anisotropy of the cluster. This is in strong analogy to what occurs in MNP, in which the magnetic anisotropy is higher than the bulk one and is modified in both strength and symmetry by the surface.

Acknowledgements

The financial support of EC through MOLSPINQIP (STREP 211284), of Italian MiUR, of Ente CRF and of the DFG Center for Functional Nanostructures is gratefully acknowledged. We thank Prof. Jinkui Tang for resynthesizing and crystallizing the sample and Mr. Paolo Parri for creating the inside cover artwork.

References

1 M. Fittipaldi, L. Sorace, A.-L. Barra, C. Sangregorio, R. Sessoli and D. Gatteschi, *Phys. Chem. Chem. Phys.*, 2009, **11**, 6555–6568.
2 W. Wernsdorfer, *Adv. Chem. Phys.*, 2001, **118**, 99–190.
3 W. Andrä and H. Nowak, *Magnetism In Medicine - a Handbook*, Wiley-VCH, 1998, p. 629.
4 M. Takafuji, S. Ide, H. Ihara and Z. H. Xu, *Chem. Mater.*, 2004, **16**, 1977–1983.
5 D. W. Elliott and W. Zhang, *Environ. Sci. Technol.*, 2001, **35**, 4922–4926.
6 A. K. Gupta and M. Gupta, *Biomaterials*, 2005, **26**, 3995–4021.
7 T. Hyeon, *Chem. Commun.*, 2003, 927–934.
8 S. Laurent, D. Forge, M. Port, A. Roch, C. Robic, L. Vander Elst and R. N. Muller, *Chem. Rev.*, 2008, **108**, 2064–2110.
9 A.-H. Lu, E. L. Salabas and F. Schüth, *Angew. Chem., Int. Ed.*, 2007, **46**, 1222–1244.
10 A.-H. Lu, W. Schmidt, N. Matoussevitch, H. Bönnemann, B. Spliethoff, B. Tesche, E. Bill, W. Kiefer and F. Schüth, *Angew. Chem., Int. Ed.*, 2004, **43**, 4303–4306.
11 (*a*) J. Connolly, Q. A. Pankhurst, S. K. Jones and J. Dobson, *J. Phys. D: Appl. Phys.*, 2003, **36**, R167–R181; (*b*) Q. A. Pankhurst, N. K. T. Thanh, S. K. Jones and J. Dobson, *J. Phys. D: Appl. Phys.*, 2009, **42**, 224001.
12 S. Taketomi, S. Chikazumi, M. Ukita, M. Mizukami, H. Miyajima, M. Setogawa and Y. Kurihara, *J. Magn. Magn. Mater.*, 1987, **65**, 245–251.
13 T. Shinjo, *Nanomagnetism and Spintronics*, Elsevier, 2009, pp. 53114–53114.
14 A. J. Tasiopoulos, A. Vinslava, W. Wernsdorfer, K. A. Abboud and G. Christou, *Angew. Chem., Int. Ed.*, 2004, **43**, 2117–21.
15 M. Su, S. Cavallo, S. Stefanini, E. Chiancone and N. D. Chasteen, *Biochemistry*, 2005, **44**, 5572–8.
16 D. J. Price, F. Lionti, R. Ballou, P. T. Wood and A. K. Powell, *Philos. Trans. R. Soc. London, Ser. A*, 1999, **357**, 3099–3118.
17 N. Hoshino, A. M. Ako, A. K. Powell and H. Oshio, *Inorg. Chem.*, 2009, **48**, 3396–407.
18 A. Bino, M. Ardon, D. Lee, B. Spingler and S. J. Lippard, *J. Am. Chem. Soc.*, 2002, **124**, 4578–4579.
19 A. K. Powell, S. L. Heath, D. Gatteschi, L. Pardi, R. Sessoli, G. Spina, F. Del Giallo and F. Pieralli, *J. Am. Chem. Soc.*, 1995, **117**, 2491–2502.
20 J. C. Goodwin, R. Sessoli, D. Gatteschi, W. Wernsdorfer, A. K. Powell and S. L. Heath, *J. Chem. Soc., Dalton Trans.*, 2000, 1835–1840.
21 E. Ruiz, A. Rodrìguez-Fortea, J. Cano and S. Alvarez, *J. Phys. Chem. Solids*, 2004, **65**, 799–803.
22 M. Affronte, J. Lasjaunias, W. Wernsdorfer, R. Sessoli, D. Gatteschi, S. Heath, A. Fort and A. Rettori, *Phys. Rev. B*, 2002, **66**, 1–7.
23 C. J. H. Jacobsen, E. Pedersen, J. Villadsen and H. Weihe, *Inorg. Chem.*, 1993, **32**, 1216–1221.
24 S. Stoll and A. Schweiger, *J. Magn. Res.*, 2006, **178**, 42–55.
25 P. Ceci, E. Chiancone, O. Kasyutich, G. Bellapadrona, L. Castelli, M. Fittipaldi, D. Gatteschi, C. Innocenti and C. Sangregorio, *Chem.: Eur. J.*, 2010, **16**, 709–717.
26 M. Fittipaldi, C. Innocenti, P. Ceci, C. Sangregorio, L. Castelli, L. Sorace and D. Gatteschi, *Phys. Rev. B*, 2011, **83**, 104409.
27 W. Demtröder, *Laser Spectroscopy*, Springer-Verlag, Berlin, 1981.
28 A. Abragam and B. Bleaney, *Electron Paramagnetic Resonance of Transition Ions*, Clarendon Press, Oxford, 1970.
29 A. Bencini and D. Gatteschi, in *Volume I*, edited by E. I. Solomon And A. B. P. Lever, (1999), pp. 93–159.
30 A. Bouwen, A. Caneschi, D. Gatteschi, E. Goovaerts, D. Schoemaker, L. Sorace and M. Stefan, *J. Phys. Chem. B*, 2001, **105**, 2658–2663.
31 C. Rudowicz and P. Gnutek, *Physica B*, 2009, **404**, 3582–3593.
32 A.-L. Barra, A. Caneschi, A. Cornia, D. Gatteschi, L. Gorini, L.-P. Heiniger, R. Sessoli and L. Sorace, *J. Am. Chem. Soc.*, 2007, **129**, 10754–10762.
33 E. Liviotti, S. Carretta and G. Amoretti, *J. Chem. Phys*, 2002, **117**, 3361.

34 L. Margheriti, M. Mannini, L. Sorace, L. Gorini, D. Gatteschi, A. Caneschi, D. Chiappe, R. Moroni, F. Buatier de Mongeot, A. Cornia, F. M. Piras, A. Magnani and R. Sessoli, *Small*, 2009, **5**, 1460–1466.
35 A.-L. Barra, P. Debrunner, D. Gatteschi, C. E. Schulz and R. Sessoli, *Europhys. Lett.*, 1996, **35**, 133–138.
36 D. Zipse, J. M. North, N. S. Dalal, S. Hill and R. S. Edwards, *Phys. Rev. B*, 2003, **68**, 184408.
37 K. Park, M. Novotny, N. Dalal, S. Hill and P. Rikvold, *Phys. Rev. B*, 2001, **65**, 8–12.
38 A. M. Ako, V. Mereacre, Y. Lan, W. Wernsdorfer, R. Clérac, C. E. Anson and A. K. Powell, *Inorg. Chem.*, 2010, **49**, 1–3.
39 H. Li, M. Klem, K. Sebby, D. Singel, M. Young, T. Douglas and Y. Idzerda, *J. Magn. Magn. Mater.*, 2009, **321**, 175–180.
40 R. J. Usselman, M. T. Klem, M. Allen, E. D. Walter, K. Gilmore, T. Douglas, M. Young, Y. Idzerda and D. J. Singel, *J. Appl. Phys.*, 2005, **97**, 10M523.
41 N. Noginova, F. Chen, T. Weaver, E. Giannelis, A. Bourlinos and V. Atsarkin, *J. Phys.: Cond. Matt.*, 2007, **19**, 246208.
42 N. Noginova, T. Weaver, E. Giannelis, A. Bourlinos, V. Atsarkin and V. Demidov, *Phys. Rev. B*, 2008, **77**, 1–5.
43 J. Kliava and R. Berger, in *Smart Materials For Ranging Systems* Edited by J. Franse, V. Eremenko And V. Sirenko, NATO Science Series II, Springer, 2006, pp. 27–48.
44 R. J. Usselman, M. T. Klem, S. E. Russek, M. Young, T. Douglas and R. B. Goldfarb, *J. Appl. Phys.*, 2010, **107**, 114703.
45 M. Noginov, N. Noginova, O. Amponsah, R. Bah, R. Rakhimov and V. Atsarkin, *J. Magn. Magn. Mater.*, 2008, **320**, 2228–2232.
46 A. Bencini and D. Gatteschi, *EPR of Exchange Coupled Systems*, Springer-Verlag, Berlin, 1990.
47 A. Cornia, M. Affronte, A. G. M. Jansen, G. L. Abbati and D. Gatteschi, *Angew Chem. Int. Ed.*, 1999, **38**, 2264–2266.
48 A.-L. Barra, A. Caneschi, A. Cornia, F. Fabrizi, De Biani, D. Gatteschi, C. Sangregorio, R. Sessoli and L. Sorace, *J. Am. Chem. Soc.*, 1999, **121**, 5302–5310.
49 E. Tancini, M.-J. Rodriguez-Douton, L. Sorace, A.-L. Barra, R. Sessoli and A. Cornia, *Chem. Eur. J.*, 2010, **16**, 10482–10493.
50 D. Gatteschi, A. L. Barra and R. Sessoli, *Chem. Eur. J.*, 2000, **6**, 1608–1614.
51 M. Gerloch and J. Lewis, *J. Chem. Soc. A*, 1969, 1422–1427.
52 G. L. Abbati, L. C. Brunel, H. Casalta, A. Cornia, A. C. Fabretti, D. Gatteschi, A. K. Hassan, A. G. M. Jansen, A. L. Maniero, L. A. Pardi and C. Paulsen, *Chem. Eur. J.*, 2001, **7**, 1796–1807.
53 D. Gatteschi, L. Sorace, R. Sessoli and A.-L. Barra, *Appl. Magn. Reson.*, 2001, **21**, 299–310.
54 M. G. Uytterhoeven, A. Bencini and I. Ciofini, *Inorg. Chim. Acta*, 1998, **274**, 90–101.
55 D. Gatteschi and L. Sorace, *J. Sol. State Chem.*, 2001, **159**, 253–261.
56 T. Moryia, in *Magnetism*, edited by G. T. Rado and H. Suhl, Academic Press, New York, 1963, p. 85.
57 P. ter Heerdt, M. Stefan, E. Goovaerts, A. Caneschi and A. Cornia, *J. Magn. Res.*, 2006, **179**, 29–37.
58 A. Ozarowski, B. R. McGarvey and J. E. Drake, *Inorg. Chem.*, 1995, **34**, 5558–5566.